Surface Characterization of PBO Fibers

Katia Tamargo-Martínez, Silvia Villar-Rodil, Juan I. Paredes, Amelia Martínez-Alonso, Juan M. D. Tascón, and Miguel A. Montes-Morán*

Instituto Nacional del Carbón, CSIC, Apartado 73, 33080 Oviedo, Spain

Received April 23, 2003; Revised Manuscript Received September 5, 2003

ABSTRACT: We report on the surface characterization of commercial poly(*p*-phenylene benzobisoxazole) (PBO) fibers. Several solvents (hexane, acetone, and ethanol) were employed to remove the sizing present on the fiber surfaces. The surface properties of the different samples were studied by means of inverse gas chromatography (IGC) at infinite dilution using nonpolar *n*-alkanes and molecules with different acid−base characteristics (benzene, pyridine, acetonitrile, nitromethane, *tert*-butyl alcohol). Complementary information was obtained by using thermogravimetric/differential thermal analysis (TG/DTA) and atomic force microscopy (AFM). Results showed that, whereas the sizing of high-modulus (HM) fibers can be gradually washed off as the polarity of the solvent increases, only ethanol washing allowed to detect changes in the surface characteristics of PBO as-spun (AS) fibers, with hexane and acetone having little or no effect. In fact, it is believed that the effect of any coating applied eventually to the PBO AS fibers is masked by the presence of poly(phosphoric acid) (PPA) or partially coagulated PPA/PBO residuals on their surfaces, which in turn determine their surface properties. In any case, both standard finishes and contaminants strongly decrease the surface energy of the PBO fibers. According to the experimental results, it was assumed that PBO pristine fiber surfaces could be obtained by ethanol washing. Further differences were found between the cleaned AS and HM fibers. AFM measurements showed microfibrils present in the HM fibers that are somewhat wider than their AS counterparts. The presence of voids at the surface level of the cleaned PBO AS fibers brought about strong changes in adsorption energetics. No such changes were detected in the case of cleaned HM fibers. The contaminants of the AS fibers confer them a more acidic character than that of the rest of samples studied. Sizing/contaminants removal on both fiber types leads to an increase in the number or strength of basic sites. However, the cleaned fibers kept an amphoteric character based on the strong specific interactions existing between pyridine and the fiber surfaces. Ab initio calculations carried out on an appropriate model confirmed the presence of positively charged carbon atoms in the PBO monomers which should act as electron acceptors. Moreover, PBO fibers are prone to exert important $\pi-\pi$ interactions as it was found both experimentally (relatively high $-\Delta H_a^{SP}$ values of benzene) and predicted from the charge distribution obtained from theoretical calculations.

1. Introduction

More than 20 years ago, the US Air Force (USAF) sponsored and participated in a specific polymer program for the development of new structural materials with outstanding mechanical properties.[1,2] Various so-called rigid-rod polymers were then investigated, particularly poly(*p*-phenylene benzobisoxazole) or PBO:

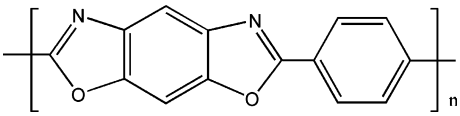

Fibers obtained from this rigid-rod polymer exhibit remarkable specific strength and modulus, cut and abrasion resistance, and long-term retention of their properties at relatively high temperatures.[3,4]

Apart from their use as such, PBO fibers can be employed as reinforcement in organic matrix composites.[5] Additionally, the excellent properties offered by PBO make this polymer a suitable matrix in more sophisticated systems, such as PBO/single-wall carbon nanotubes composites.[6] It is well established that the characteristics of the reinforcement/matrix interface are a key factor for the performance of composites. For example, a good level of adhesion is required to transfer external loads effectively from the matrix to the fibers. Although composite design involves numerous factors, it seems necessary to characterize the thermodynamic and chemical properties of the fiber surface as well as to determine the effect of these surface characteristics on the final response of the material. Fiber producers understand the relevance of such knowledge, devoting substantial research to characterize and modify the surface properties of these materials.[7]

The manufacturing process of most man-made fibers, including PBO, involves a latter stage in which fibers are coated with a thin layer of so-called sizing or finish. The main function of these sizings is to prevent the individual filaments of a fiber tow from contact damage between themselves or from eyelets or guides during weaving or prepregging. Additionally, many commercial sizings are formulated to be multifunctional, i.e., to promote adhesion between the fiber and a given matrix. Sizings are thus critical in composite manufacturing and may have or have not positive effects on the final properties of the composite material.[8] As just mentioned, the process is fully implemented in PBO fiber production lines, and it is fairly rare to obtain sizing- or finish-free fibers commercially, i.e., fibers with no coating on their surfaces. Thus, solvents of different polarity should be used in order to obtain "clean" PBO surfaces. The effect of such a solvent extraction on the final properties of the fibers is also an important subject of investigation.[9]

* Corresponding author: e-mail miguel@incar.csic.es; Tel + 34 985 11 90 90; Fax + 34 985 29 76 62.

10.1021/ma034522l CCC: $25.00
Published on Web 10/23/2003

Table 1. Elemental Analyses (wt %) of As-Received PBO Fibers (Dry Basis)

fiber	C	H	N	S	O
PBO AS	70.91	2.85	12.00	0.0	14.91
PBO HM	71.42	2.54	12.20	0.0	14.46
theoretical prediction	71.78	2.58	11.96		13.66

In this paper, adsorption of relevant probes on different PBO fiber surfaces was studied by means of inverse gas chromatography (IGC). IGC constitutes an ideally suited technique to study adsorption at very low coverage (infinite dilution) and has demonstrated its usefulness for the surface characterization of a wide range of materials, especially polymers.[10−15] Other characterization techniques such as thermogravimetry/differential thermal analysis (TG/DTA) and atomic force microscopy (AFM) were also employed.

2. Experimental Section

2.1. Materials. The PBO fibers used in this study were in the form of Zylon (Toyobo, Japan). The two starting samples were as-spun PBO fiber Zylon AS 555 dtex (subsequently referred to as sample AS in this work) as well as its high-modulus version Zylon HM 545 dtex (referred to as sample HM). The high-modulus PBO fiber is prepared after the heat treatment (at approximately 800 K) under tension of the as-spun fiber. This posttreatment is intended to improve the mechanical properties of the PBO fiber. Thus, typical values of the fibers tensile strength and modulus after the heat treatment are correspondingly 5.8 and 270 GPa, whereas values of 4.8 and 180 GPa are obtained for the AS fibers, respectively. Manufacturer filament diameter values were approximately 12 and 11 μm for the AS and HM PBO fibers, respectively. Elemental analyses of the as-received fibers were carried out in a LECO CHNS-932 microanalysis apparatus with a LECO VTF-900 accessory for oxygen. Results, which are collected in Table 1, agree well with the theoretical prediction for a pristine PBO material.

These two commercial PBO fibers were supplied coated with a proprietary sizing or finish. Different solvents of increasing polarity, namely *n*-hexane, acetone, and ethanol, were employed to remove that sizing from the PBO surfaces. Thus, yarns of AS and HM fibers were thoroughly washed with each solvent, and samples prepared in such a way were labeled as -hex, -acet, -etOH. Yarns of the AS sample Soxhlet-extracted in acetone for 60 cycles were also characterized for comparative purposes (see Results and Discussion).

2.2. Methods. Adsorption measurements were carried out by IGC at infinite dilution using a Hewlett-Packard 5890-II gas chromatograph equipped with a high sensitivity (10^{-12} mol) flame ionization detector. Continuous fiber yarns (0.7−1 g) were packed into approximately 40 cm long passivated nickel columns (2.31 mm i.d.). Helium (99.9995% pure) was used as carrier gas. The gas flow rate F (15−20 mL min^{-1}) was measured at the column outlet (F_{flo}) by using a bubble flowmeter. Corrections were made for temperature difference between the column (T) and the flowmeter (T_{flo}), water vapor pressure of the bubble (P_w), and pressure drop (j correction factor, with P_{out} and P_{in} being the pressure at the outlet and inlet, respectively):[16]

$$F = jF_{flo}\frac{T}{T_{flo}}\left[\frac{P_{out} - P_w}{p_{out}}\right] \quad (1)$$

$$j = \frac{3}{2}\left[\frac{(P_{in} - P_{out})^2 - 1}{(P_{in} - P_{out})^3 - 1}\right] \quad (2)$$

Adsorption experiments were carried out at 10 K intervals in the 303−343 ± 0.05 K temperature interval. Small amounts (0.1−1 μL) of vapors of *n*-alkanes (C_7−C_{12}, >99% pure) measured with a 10 μL Hamilton syringe were eluted through the columns. Changes in the surface chemistry were evaluated by injecting several polar probes of different acid−base characteristics (benzene, nitromethane, acetonitrile, pyridine, *tert*-butyl alcohol, purity >99%). At least five injections of each probe were carried out at each temperature. No variation was detected in the retention volume of the probes when different flow rates were used. This indicates that adsorption equilibrium was attained.[16] Prior to the IGC experiments, the chromatographic columns were conditioned by heating at 373 K under a constant helium flow (∼20 mL min^{-1}). Typical conditioning times of 12 h were necessary to achieve reproducible results. The helium flow through the columns was not interrupted anytime in the course of the experiments in order to prevent further contamination of the fibers after column conditioning.

A Stanton-Redcroft STA-1500 thermobalance provided with Plus-V software was used for simultaneous thermogravimetry (TG)/differential thermal analysis (DTA) measurements. In all thermal treatments, as-received fibers were used without previous drying. Samples (∼25 mg) were placed in Pt crucibles 5 mm in diameter and 5 mm in height. Constant argon and air (99.999% pure by volume) flows of 50 cm^3 min^{-1} were respectively used in pyrolysis and oxidation experiments. Temperatures were measured with Pt/Rh thermocouples placed at the bottom of the Pt crucibles, in contact with them. α-Alumina was the reference material for DTA measurements. For all the experiments, both in inert atmosphere and in air, the sample was heated at a linear heating rate of 10 K min^{-1} to 703 K, the temperature at which it was kept for 30 min.

The PBO samples were also investigated by atomic force microscopy (AFM) in the tapping mode of operation. The AFM observations were carried out in air at room temperature with a Nanoscope Multimode IIIa (Digital Instruments) apparatus. Rectangular silicon cantilevers with spring constants of about 40 N m^{-1} and resonance frequencies around 250 kHz were employed. Their nominal tip radius of curvature was 5−10 nm. Bundles of fibers were attached to sample holders by means of double-sided carbon adhesive tape, paying special attention to avoid the presence of fibers sticking out of the sample surface, which could prevent the attaining of a stable and valid AFM signal. Imaging was accomplished in the intermittent contact regime,[17] with free and set point amplitudes of cantilever oscillation of about 75 and 68 nm, respectively. To detect the presence of possible contaminant layers on the PBO fiber surface, phase contrast images were acquired concurrently with the regular, topographical ones. Likewise, to check that the recorded images were reproducible and representative of the investigated samples, several different and previously unused probes were employed, many different fibers of every PBO sample were inspected, and each fiber was imaged at many different locations.

The XPS spectra were recorded with a triple channeltron CLAM-2 analyzer using Al Kα radiation under an operating vacuum better than 3×10^{-8} mbar. Continuous yarns of the different fibers were rolled on silver stubs and clamped using a metallic clip. Wide scan spectra were taken at a constant analyzer transmission energy of 100 eV. Surface atomic compositions were calculated from the areas of relevant peaks from survey scan spectra after fitting of a Shirley background. Binding energy (BE) values were charge-corrected to the C 1s signal, which was set at 284.6 eV. BE values have an accuracy of 0.2 eV.

To characterize the molecular structure and charge distribution of PBO monomer-like compounds, quantum chemical calculations were carried out using the Gaussian98 suite of programs.[18] The level of theory used in this work combines a density functional theory (DFT) method, the B3LYP hybrid functional corresponding to Becke's three-parameter exchange functional with the Lee−Yang−Parr gradient-corrected correlation functional,[19] with the 6-31G* basis set which is double-ζ augmented with one set of polarization functions on heavy atoms.[20] A full geometry optimization of a PBO monomer model was performed using redundant internal coordinates with no constraints. Atomic charges were computed

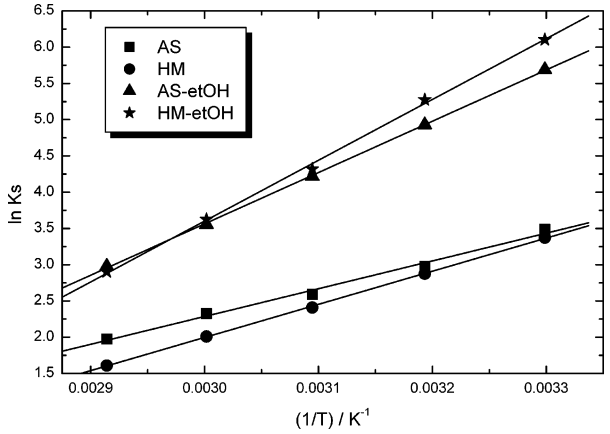

Figure 1. Variation of (ln *Ks*) with (1/*T*) for the adsorption of *n*-nonane on PBO AS samples.

carrying out a natural population analysis (NPA) on the corresponding B3LYP/6-31G* density matrix.[21]

3. Results and Discussion

Unlike conventional adsorption techniques, IGC allows the measurement of adsorption data down to very low vapor concentrations, where the surface coverage approaches zero and adsorbate−adsorbate interactions are negligible. The chromatographic peaks obtained for the *n*-alkanes were mainly symmetrical for all samples under study, with no dependence of the peak maximum position on the amount of probe molecule injected. Under these conditions the adsorption can be considered to take place in the linear part of the isotherm (Henry's law), and the retention time of the different *n*-alkanes could be measured at the peak maximum.[16] The Henry's law constant, K_s, which characterizes the adsorption equilibrium, is related directly to the retention volume by

$$V_N = K_s A \tag{3}$$

where A is the total surface area of the stationary phase. The previous equation is valid as long as the bulk absorption of the probe in the stationary phase is negligible.[16] Thermodynamic functions of the adsorption process at infinite dilution can thus be calculated from K_s. Details for calculating the standard free energy of adsorption, ΔG_a^0, standard entropy, ΔS_a^0, and heat of adsorption, q_d^0, are given elsewhere.[22] Since CO_2 adsorption isotherms performed on the as-received samples at 273 K were found to be linear and with very low adsorption capacity (results not shown), the specific surface area of the PBO AS and PBO HM fibers was assumed to be equal to the specific geometric area, as calculated from fiber diameter values of 12.3 and 11.2 μm, respectively.

Figure 1 illustrates the linear dependence of ln K_s as a function of (1/*T*) obtained for the adsorption of *n*-nonane on the different PBO samples. This behavior, which is extensive to the rest of the *n*-alkane−adsorbent systems, implies that q_d^0 is constant within the studied temperature range. The standard deviations in q_d^0 values obtained in this way were never larger than 2%. Values of the differential heats of adsorption at zero coverage of *n*-alkanes on all PBO fibers under study are given in Tables 2 and 3.

In agreement with the linearity in ln K_s vs (1/*T*) plots (Figure 1), the adsorption entropies ΔS_a^0 were independent of temperature. Values of ΔS_a^0 given in Tables 4 and 5 are the average of data calculated at the different temperatures, deviations being smaller than 1%.

Table 2. Differential Heats of Adsorption of *n*-Alkanes on the PBO AS Samples

	q_d^0 (kJ mol^{-1})				$-\Delta H_{Liq}$[a]
n-alkane	AS	AS-hex	AS-acet	AS-etOH	(kJ mol^{-1})
C_7		22.5	22.1	55.6	35.0
C_8	25.7	26.7	26.9	61.0	39.8
C_9	31.8	31.8	33.3	71.8	44.6
C_{10}	37.6	37.7	40.1	72.0	49.4
C_{11}	44.3	44.1	47.4		54.2
C_{12}	47.6	45.5			58.9

[a] Heats of liquefaction (kJ mol^{-1}).

Table 3. Differential Heats of Adsorption of *n*-Alkanes on the PBO HM Samples

	q_d^0 (kJ mol^{-1})				$-\Delta H_{Liq}$[a]
n-alkane	HM	HM-hex	HM-acet	HM-etOH	(kJ mol^{-1})
C_7			41.7	45.0	35.0
C_8	34.9	42.1	47.3	51.5	39.8
C_9	38.0	47.1	54.3	58.1	44.6
C_{10}	42.0	52.5	61.3	65.3	49.4
C_{11}	45.9	57.0	68.7	69.6	54.2
C_{12}	49.5	61.7			58.9

[a] Heats of liquefaction (kJ mol^{-1}).

Table 4. Standard Entropies of Adsorption of *n*-Alkanes on the PBO AS Samples

	$-\Delta S_a^0$ (J K^{-1} mol^{-1})				$-\Delta S_a^0$[a]
n-alkane	AS	AS-hex	AS-acet	AS-etOH	(J K^{-1} mol^{-1})
C_7		14.8	13.8	109.4	52.4
C_8	18.0	19.8	20.7	114.1	53.0
C_9	29.1	27.8	32.4	137.7	53.5
C_{10}	39.0	38.1	46.0	129.2	53.9
C_{11}	51.9	50.2	59.9		54.3
C_{12}	52.0	47.2	60.0		54.7

[a] Standard entropy of adsorption (at 303 K) calculated according to de Boer's model.[26]

Table 5. Standard Entropies of Adsorption of *n*-Alkanes on the PBO HM Samples

	$-\Delta S_a^0$ (J K^{-1} mol^{-1})				$-\Delta S_a^0$[a]
n-alkane	HM	HM-hex	HM-acet	HM-etOH	(J K^{-1} mol^{-1})
C_7			67.8	77.4	52.4
C_8	47.9	70.2	75.4	87.1	53.0
C_9	50.0	77.4	86.9	97.2	53.5
C_{10}	55.1	85.1	98.2	108.7	53.9
C_{11}	59.8	90.5	110.7	111.6	54.3
C_{12}	64.0	96.2			54.7

[a] Standard entropy of adsorption (at 303 K) calculated according to de Boer's model.[26]

Values of the dispersive component of the surface free energy, γ_S^D, were calculated using the formula proposed by Gray:[23]

$$\frac{-\Delta G_a^{CH_2}}{N_A a_{CH_2}} = 2(\gamma_{CH_2}\gamma_S^D)^{1/2} \tag{4}$$

where $\Delta G_a^{CH_2}$ is the difference in the free energy of adsorption of two *n*-alkanes with succeeding values of n, N_A is Avogadro's number, a_{CH_2} is the area of one methylene group (0.06 nm^2), and γ_{CH_2} is the surface tension of ideal liquid polyethylene. Figure 2 illustrates

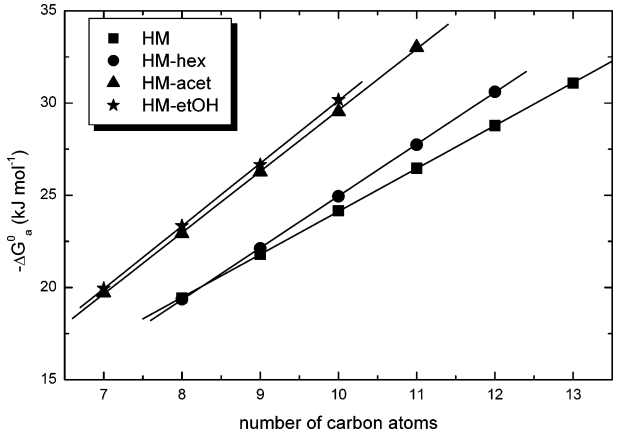

Figure 2. Variation of the standard adsorption free energy ($-\Delta G_a^0$) with the number of carbon atoms in *n*-alkanes ($-\Delta G_a^0$ data at 323 K) for the different PBO HM samples.

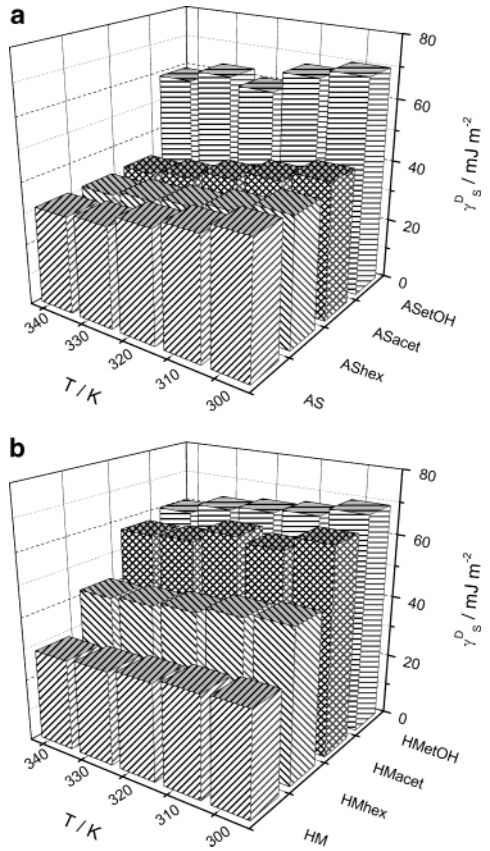

Figure 3. Dispersive component of the surface free energy of PBO fibers at various temperatures: (a) AS samples; (b) HM samples.

the linear variation of $-\Delta G_a^0$ (at 323 K), for the PBO HM samples, with the number of carbon atoms in the series of *n*-alkanes used as probes. Similar correlations were obtained for the rest of fibers under study. The slope of the regression lines corresponds to $-\Delta G_a^{CH_2}$ for the different samples, at a given temperature. Calculated γ_S^D values are plotted in Figure 3 for the various PBO fibers within the range of temperatures studied. As mentioned in the case of other thermodynamic magnitudes, uncertainties in γ_S^D values are very small (1−2%) due to the excellent data correlations obtained, similar to those shown in Figure 2.

Hitherto in this work, the values of the thermodynamic magnitudes reported for the two commercial Zylon fibers (AS and HM samples) are paradigmatic of sized fibers. Similar γ_S^D values have been obtained, for example, for poly(*p*-phenylene terephthalamide) (PPTA) fibers and carbon fibers commercially coated with different substances.[22,24] The information provided by IGC at infinite dilution mainly concerns the interaction of the vapor probes with the low surface energy constituents of the sizing. Thus, q_d^0 values of the AS and HM are lower than the heats of liquefaction ($-\Delta H_{Liq}$) of the *n*-alkanes at 323 K (also listed in Tables 2 and 3). The complete isotherm of adsorption of *n*-alkanes on these two PBO fibers should be type III according to the IUPAC classification.[25,26] This type of adsorption is representative of weak dispersive adsorbate−adsorbent interactions. A similar conclusion can be reached from the analysis of the standard entropies of adsorption (Tables 4 and 5). Also included in these tables are the adsorption entropy values predicted by an ideal adsorption model where the adsorbate is assumed to behave ideally as a bidimensional gas.[26] The experimental adsorption entropies are lower (in absolute value) than those predicted by the theoretical estimation for the AS and HM samples (in the latter, only for the shortest alkanes). This means that the adsorbed hydrocarbons are more disordered than as predicted by a bidimensional gas model. That positive contribution to the entropy has been assigned to mixing between the adsorbed molecules and surface contaminants.[22] It must be stressed here that the possibility of probe absorption (i.e., diffusion into the bulk material) is negligible due to the operational conditions of IGC at zero coverage.[16]

Inspection of data collected in Tables 2−5 confirms that there exist systematic differences between the thermodynamic magnitudes of adsorption measured on the AS and HM fibers, in particular for the shortest alkanes (C_8−C_{10}). In the case of the AS fiber, the adsorption of these alkanes is less exothermic, with q_d^0 values of C_{11} and C_{12} approaching to those observed in the HM fibers. Entropies are systematically lower (absolute values) when the adsorption of any of the linear alkanes tested takes place onto the AS surfaces. These trends indicate that the surface of the AS fibers is less energetic than that of the HM fibers. However, values of the dispersive component of the surface tension γ_S^D (Figure 3) contradict the previous assertion, since a significantly lower γ_S^D (30 mJ m^{-2}) was obtained for the HM fiber with respect to the AS fiber (40 mJ m^{-2}) at 300 K. As mentioned in the Experimental Section, these results were reproducible in all the experiments performed with several chromatographic columns filled with AS and HM fibers. In previous work,[22] we also reported discrepancies between the changes of thermodynamic magnitudes of adsorption and γ_S^D values after a plasma treatment was carried out on PPTA fibers. A possible explanation to these observations stands on the fact that the model adopted to calculate γ_S^D (eq 4) is rather simplistic. Jagiello et al. have pointed out that the $\Delta G_a^{CH_2}$ parameter, which accounts for the differences in γ_S^D of AS and HM fibers, not only is affected by changes in surface microstructure but is also sensitive to variations in surface chemistry.[27]

Nevertheless, the relevant aspect from the point of view of the fiber surface is that the PBO AS and HM varieties behave differently. This fact should explain the differences observed in the performance of the three solvents used to clean the sizing off the fibers, as shown

by IGC measurements. The tendency of all thermodynamic magnitudes agrees now in demonstrating that only ethanol has a significant influence in the surface properties of the AS fibers, as depicted graphically in Figure 3a. Fiber HM, on the other hand (Figure 3b), is responsive to all solvents employed, which affect the fiber surface gradually more as the solvent polarity increases. A similar behavior has been previously reported for PPTA fibers subjected to solvent extraction by different solvents in order to remove their surface contaminants (sizing).[28,29] We have also demonstrated recently that acetone washing is able to clean commercial Kevlar 29 (DuPont de Nemours Intl. S.A.) fibers, rendering fiber surfaces with properties quite similar to those of pristine, unsized, PPTA fibers.[22] Thus, we found rather surprising that both hexane and, especially, acetone were ineffective at cleansing the PBO AS fibers. Moreover, yarns of the AS sample Soxhlet-extracted in acetone for 60 cycles were also analyzed after questioning the efficiency of the on-column washing. The results obtained, however, were almost identical.

Two possible factors may be responsible for the differences observed between the AS and HM fibers, i.e., (i) different sizing formulations and (ii) similar formulations but different sizing amount or spreading ability (due, for example, to different processing conditions of the two fibers). The second hypothesis was considered on the basis of previous studies concerning the effect that different sizing amounts (but same formulation) have on the surface properties of carbon fibers.[24]

The sizing or finish content is defined as the percent of the total strand weight made up by the external coating, and it is usually determined either by dissolving the organic sizing or by burning it off (also known as loss on ignition).[8] However, the use of an oxidizing atmosphere at relatively high temperatures might render misleading results when determining the sizing content of polymeric fibers due to eventual degradation of the raw material. To evaluate this possible effect on the TG/DTA behavior of PBO AS and PBO HM in air atmosphere, pyrolysis of the sized PBO samples was also performed under argon at the same conditions (see Experimental Section). Figures 4 and 5 show TG and DTA curves, respectively, of PBO HM and PBO AS samples treated under argon and air atmospheres. Moisture release is observed for AS fibers in the two corresponding curves. Whereas HM sample barely loses weight in the temperature range from 350 to 450 K (∼0.5%), AS sample loses ∼2% in the same temperature interval. This weight loss in the AS sample is accompanied by an endothermal effect in the DTA curve with a minimum at approximately 300 K. The moisture remaining in this sample should be ascribed to the processing conditions of the AS fibers, which are dry-jet wet spun through air into an aqueous solution (typically water).[2] The heat posttreatment devoted to improve the modulus of the fiber, i.e., to obtain the HM sample used in the present study, should also reduce significantly that residual moisture. Apart from their moisture content, the two types of fibers are clearly distinguished by the appearance of a weak exothermal effect around 490 K in the DTA curve for HM sample, accompanied by a small step of ∼0.3 wt % in the TG curve, for the treatment in air. This step is shifted to higher temperatures (∼600 K) in the case of the thermal treatment carried out in an argon atmosphere. AS fibers

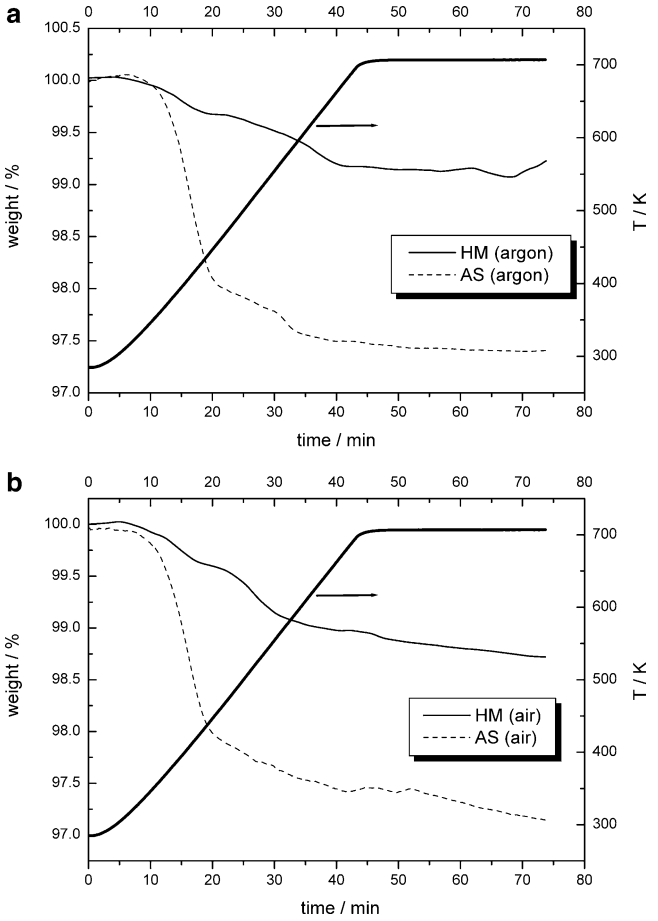

Figure 4. TG curves for the pyrolysis of as-received PBO AS and HM fibers in (a) argon and (b) air atmospheres. Also included is the temperature−time profile (thick line).

also experience some weight loss after the end of the moisture release in both types of treatment: in inert atmosphere there is a slight continuous weight loss from 450 K, followed by a small step (∼0.2%) at around 560 K; in air, no step is observed but a gradual weight loss remains, without any clear DTA effect accompanying it. From these results, it is apparent that AS and HM fibers have different sizings. However, it might be argued that the small weight loses observed in the TG experiments carried out with the AS fiber, similar to those observed for the HM fibers, could be due to the existence of capillary water adsorbed into the as-spun fibers. Indeed, the use of differential scanning calorimetry and solid-state NMR have demonstrated that significant amounts of water are packed into capillary voids whose diameter is around 2−3 nm.[30] Whereas the presence of such water would be minimized after the heat treatment performed to obtain the HM fibers, significant quantities could remain absorbed in the as-spun fibers. Release of this capillary water during the thermogravimetric analysis of the AS fibers at temperatures from 400 to 500 K could mask any exothermal effect associated with the burning of the sizing constituents. Thus, the possibility that AS and HM fibers possess the same type of sizing cannot be discarded without further analysis.

PBO HM and AS samples were dried overnight under vacuum at 383 K and then subjected to the heat treatments under Ar and air atmospheres described already. No endothermal effect was found in the DTA curves for the AS fiber heated under inert atmosphere,

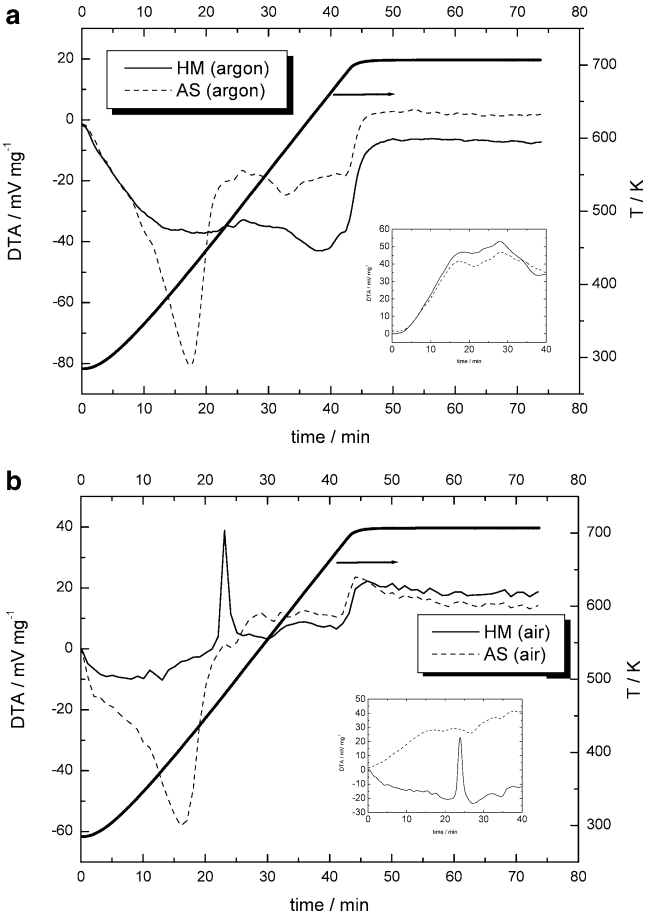

Figure 5. DTA curves for the pyrolysis of as-received PBO AS and HM fibers in (a) argon and (b) air atmospheres. Also included is the temperature−time profile (thick line). The small boxes correspond to the results obtained after drying the fibers under vacuum at 383 K (see text).

neither in the range of ordinary moisture nor in a higher temperature range (see Figure 5a). Thus, moisture and capillary water (if present) must have been eliminated. If some endothermal effect connected with capillary water had been the cause for the disappearance of an exothermal effect in treatments under air for the as-received AS fiber, this exothermal effect should be visible now that the capillary water has been eliminated. This is not the case: no exothermal effect is observed for air-treated AS fiber (see Figure 5b), and the difference between the two varieties persists in the DTA curves obtained after treatments in air. Therefore, we may conclude that the coatings of the two commercial fibers are different.

As a subsequent stage in the present investigation, AFM imaging was carried out to disclose the PBO fiber nanostructure and provide visual information on the possible presence of extraneous material on its surface. First, several AFM images of the PBO AS fiber are presented in Figure 6. The typical appearance of the surface of this sample is evidenced in parts a and b of Figure 6, where height (i.e., topography) and corresponding phase contrast images are respectively shown. According to its phase behavior (Figure 6b), the sample surface consists mainly of two well-differentiated types of regions or domains, which are observed as bright and dark areas in the phase image. It is also noticed that the bright domains of this image correspond invariably to raised areas (∼5 nm) in the height image (Figure 6a). Furthermore, the bright (raised) domains in the phase (height) image appear essentially structureless, whereas the dark areas of the phase image, which correspond to lower-lying areas in the height image, display a microfibrillar conformation. The microfibrils are arranged parallel to the top−bottom direction in all the images, i.e., along the fiber axis direction. The microfibrillar structure can be best appreciated in Figure 6c, which presents a more detailed height image. From this and similar images, the microfibrils were measured to be 10−15 nm wide, stretching parallel to the fiber axis over several tens of nanometers. Taking into account all these observations, we conclude that the bright, structureless domains of the phase images result from a contaminant layer on the PBO AS surface, while the dark, microfibrillar regions correspond to the fiber surface itself. This kind of microfibrillar structure is quite typical of polymeric fibers and is thought to reflect their molecular conformation, where the polymer chains are more or less aligned parallel to the fiber axis.[22] It should be also mentioned that, as roughly estimated from the AFM images, about 50% of the PBO AS fiber surface was covered by the contaminant layer.

Figure 7 presents a set of images analogous to the previous one [height (a) and matching phase contrast (b) images and (c) detailed height image], but in this case corresponding to the PBO HM fiber. It is noted that some differences exist between this and the AS fiber. As opposed to the latter, on the HM sample the bright areas in the phase images (Figure 7b), which are also interpreted as contaminants, do not form more or less continuous layers, but rather appear as small patches or spots (15−40 nm large). Although the patches/spots are quite numerous, a significant fraction of surface is free of them, and so the detailed HM structure can be revealed (Figure 7c). Microfibrils are also seen on this

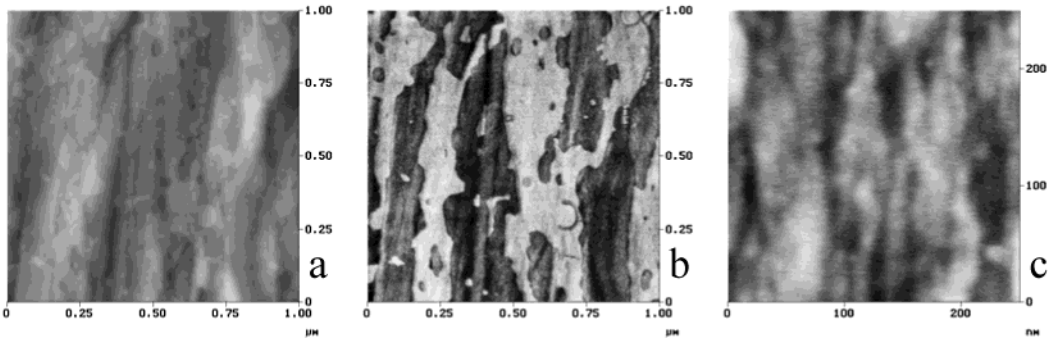

Figure 6. (a) Typical tapping mode AFM height and (b) corresponding phase contrast images of the as-received PBO AS fiber surface. (c) Higher resolution height image showing the fiber structure in detail.

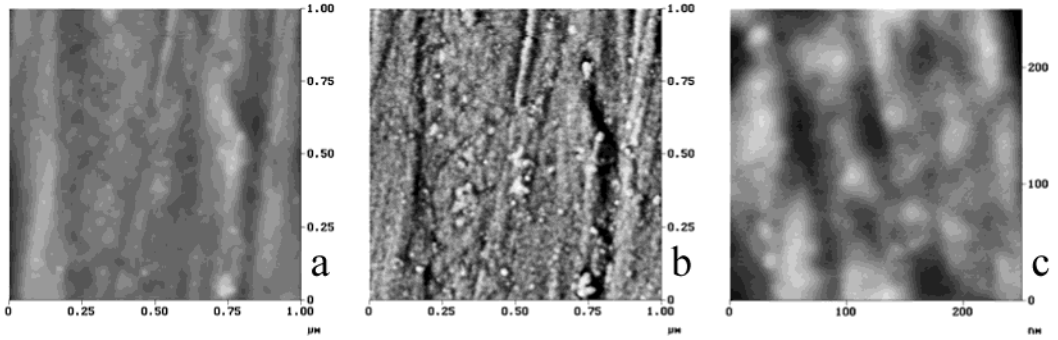

Figure 7. (a) Tapping mode AFM height and (b) corresponding phase contrast images of as-received PBO HM fibers. (c) Detailed height image of the fiber.

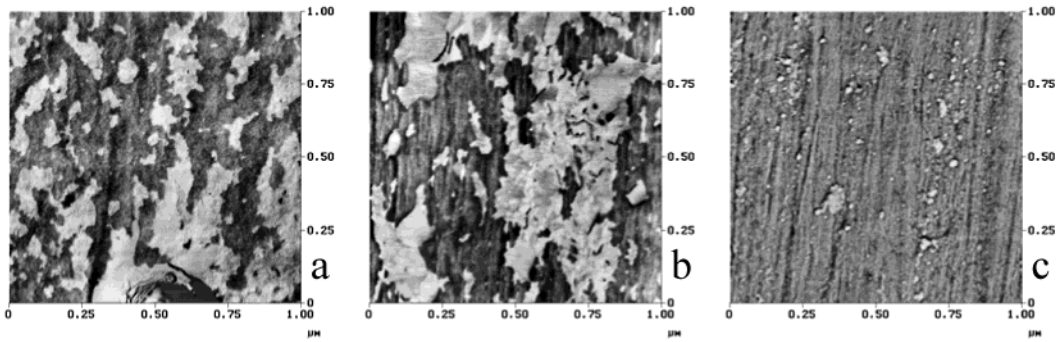

Figure 8. (a) Tapping mode phase contrast images of the PBO AS fiber samples washed with acetone by the Soxhlet method, (b) annealed at 380 K for 11 h, and (c) washed on-column with ethanol.

fiber, but they turn out to be somewhat wider (15−20 nm) than their AS counterparts.

Next, AFM was used to examine the efficiency of different procedures that were implemented in order to get rid of the contaminant layer on the PBO AS fiber surface. Figure 8 shows phase images obtained from samples (a) Soxhlet-washed with acetone and (c) on column-washed with ethanol; additionally, yarns of AS fibers annealed at 380 K for 12 h were also analyzed to evaluate the effect of the chromatographic pretreatment (see Experimental Section) on the fiber surfaces (Figure 8b). The phase images indicated that the first two methods (Figure 8a,b) were ineffective in removing the layer, since no essential changes relative to the as-received AS sample (Figure 6b) were found in this regard. By contrast, when ethanol was employed as washing agent (Figure 8c), the layer was almost completely wiped out, and there only remained small patches and spots of contaminant.

Revisiting the chromatographic results, conclusions obtained from the use of AFM should help us now to understand the differences observed during the elution of the *n*-alkanes as well as those existing between the thermodynamic magnitudes derived thereafter. The brighter areas of Figure 6b seem to determine the surface properties of the AS fibers measured by IGC. Although it could be assumed, at a first glance, that those areas consist of sizing substances, thus suggesting that the coating applied to the AS and HM fibers would be different, an alternative explanation is that the surface contaminants of Figure 6b are residues derived from the production of the PBO AS fibers. During the full coagulation of the PBO/poly(phosphoric acid) (PPA) dope in a water bath, all PPA contents are supposed to wash away.[2] However, we reckon that significant amounts of PPA or partially coagulated PBO/PPA dope remain at the surface of the as-spun fibers; i.e., the washing process is not complete. XPS analysis performed on PBO HM and AS fibers have detected phosphorus only in the surface of the as-spun fibers (Table 6). This would also explain that only ethanol is able to wipe away the bright areas in the AFM images (Figure 6b), which would correspond to the mentioned residues, since PPA is only soluble in highly polar solvents such as water and alcohols. Additionally, the effect of the sizing (if existing any) on the surface properties of the as-spun fibers cannot be determined by IGC, since the elution of the probes is governed mainly by their interaction with the PPA deposits.

Table 6. Atomic Percentages of Primary Elements (Excluding H) of Several PBO Samples

fiber	C	N	O	P
AS	77.2	4.4	17.0	1.4
HM	73.8	4.1	22.0	
et-OH washed	73.7	7.4	17.4	

Henceforth in the paper it is assumed that the on-column washing with ethanol renders almost pristine PBO fibers. XPS values of the atomic concentration at a surface level were very similar for both HM and AS fibers washed with ethanol, and they are also given in Table 6. When compared to the bulk and theoretical atomic concentrations (Table 1), the discrepancies are noticeable (lower N concentration and higher O concentration in the surface of the fibers). This may indicate that still some contaminants remain after the washing process. It has to be mentioned, however, that PPTA fibers free of sizing/finish also showed a similar level of discrepancies between both surface and bulk/theoretical atomic concentrations.[22] Nevertheless, a final aspect may be ultimately considered with regard to the IGC characterization of the AS-etOH and HM-etOH fibers using linear alkanes at zero surface coverage. Analysis

of the heats of adsorption (Tables 2 and 3) reveals that the process is more exothermic in the case of AS-etOH when compared to HM-etOH, for all alkanes tested. Entropies of adsorption (Tables 4 and 5) also corroborate this difference between the two clean fibers. Moreover, q_d^0 values of the HM-etOH sample agree with those obtained for pristine PPTA surfaces.[22] The highly energetic adsorbate−adsorbent interaction measured on the AS-etOH fibers must be related to the existence in their surface of high-energy sites which can be considered as pores or voids. It is known that the curvature of pore walls in microporous materials modifies the surface energy in comparison with that of a flat surface, resulting in a stronger, more exothermic, adsorbate−adsorbent interaction.[31,32] A similar situation has been recently reported in the case of plasma-treated PPTA fibers, where an increase of surface roughness of the plasma-treated fibers brought about an increase of the heats of adsorption of linear alkanes.[22] The porosity of the AS-etOH fibers has to be understood as the existence of voids that would only affect the adsorption of alkanes at a very low adsorbate concentration (close to zero surface coverage). Previous morphological studies on PBO fibers led to postulate a structural model for the AS fiber where microfibrils composed of highly aligned PBO molecules coexist with capillary-like microvoids.[33] Further drying (heat treatment) of the fibers brings about the removal of such structural defects, which agrees with our IGC measurements. Apart from enhancing the exothermicity of the adsorption, the existence of those voids would validate the size exclusion phenomenon which is taking place on the AS-etOH fiber. Indeed, the effect of the pore walls curvature in both q_d^0 and ΔS_a^0 drops substantially from C_9 to C_{10} (Tables 2 and 4). Hence, an estimation of the microvoids size could be also made from our IGC results, assuming that the length of the chain will be the limiting molecular dimension for the alkanes entering into the pores. This length is approximately 1.5 nm for *n*-decane,[34] which agrees reasonably well with the width of the microvoids of PBO AS fibers. This was estimated to be ∼2 nm by using Guinier's method for the equatorial streak of small-angle X-ray scattering (SAXS) patterns.[33] However, it must be mentioned here that although Kitagawa's structural model for PBO AS fiber comprises the existence of an outer fiber skin (0.2 μm thick, as measured by transmission electron microscopy) free of microvoids,[33] IGC experiments would indicate that pores persist in the very surface of the AS-etOH fiber.

The final part of the present study deals with differences in surface chemistry between the PBO fibers under examination. We have carried out IGC experiments at infinite dilution with several polar probes which were eluted through columns filled with the two as-received fibers (samples AS and HM) and the two clean fibers (samples AS-etOH and HM-etOH). The adsorption of polar molecules on the stationary phase is influenced not only by dispersive interactions as in the case of linear alkanes but also by additional specific contributions. These specific contributions include dipole−dipole and acid−base interactions (or electron acceptor−donor effects), the latter ones involving much higher energies than the former ones.[35] The ability of these polar probes to donate or accept electrons has been parametrized by means of the so-called donor number (DN) and acceptor number (AN), respectively.[35] Table 7 contains the DN and AN parameters of the probes used in this work.[35,36]

Table 7. Donor Numbers (DN) and Acceptor Numbers (AN) of the Polar Probes Used in This Work

probe	AN (kJ mol^{-1})	DN (kJ mol^{-1})
benzene	0.7	0.4
pyridine	0.6	138.5
acetonitrile	19.7	59
nitromethane	36	11.3
tert-butyl alcohol	38.1	

Table 8. Differential Heats of Adsorption (kJ mol^{-1}) of Several Polar Probes on PBO Surfaces

	AS	HM	AS-etOH	HM-etOH
benzene	26.8	29.2	44.3	27.6
pyridine	40.2	39.7	63.3	58.6
acetonitrile		30.9	42.2	38.5
nitromethane	39.0	36.6	49.9	41.5
tert-butyl alcohol	44.3	35.8	67.8	49.0

Slight concentration-dependent effects were observed for the elution of polar probes through all chromatographic columns due to the so-called "slow kinetic processes".[16] To reduce the degree of the peaks asymmetry, it was necessary to work at extremely low probe concentrations, i.e., at low signal-to-noise ratio levels. Retention times were estimated from the first momentum of peaks obtained at such conditions. Therefore, similar thermodynamic properties to those described for the elution of linear alkanes could be obtained for the polar probes injected. Plots of ln *Ks* vs (1/*T*) similar to those of Figure 1 were obtained for all polar probes. As in the case of the alkanes, reasonably good data regressions could be drawn. Values of standard enthalpies of adsorption (or differential heats of adsorption) were calculated and are given in Table 8. Standard errors are once more relatively small, approximately 2% of values collected in Table 8.

Two main components can be considered to contribute to the standard enthalpy of adsorption of polar probes, namely the specific contribution ΔH_a^{SP} and the dispersive contribution ΔH_a^{D}:[37]

$$\Delta H_a^0 = \Delta H_a^{SP} + \Delta H_a^{D} \qquad (5)$$

Several procedures have been developed in order to evaluate ΔH_a^{SP} from IGC measurements at zero surface coverage. Among them, the method proposed by Donnet et al.[38] seems to be more robust than the rest to account for the specific (acid−base) interaction of polar probes adsorbed on relatively high-energy surfaces. This method entails the estimation of $-\Delta G_a^{SP}$ from molecular polarizability data, as described elsewhere.[37,38,22] Pertinent $-\Delta G_a^{SP}$ data, at 303 K, are plotted in Figure 9.

$-\Delta H_a^{SP}$ can be now computed from the variation of $(-\Delta G_a^{SP}/T)$ vs $(1/T)$. Results obtained for the four varieties under study are collected in Table 9. Occasionally, regression of data was rather poor. Individual standard errors are therefore included (in parentheses) in Table 9. Values of $-\Delta H_a^{SP}$ will be used here to compare the acid−base character of the different PBO surfaces under study. These parameters can only account for semiquantitative changes in the surface chemistry of a given fiber. Further empirical approaches suggested by other authors would lead eventually to absolute parameters, similar to the AN and DN numbers mentioned before, describing the electron donor−acceptor properties of the

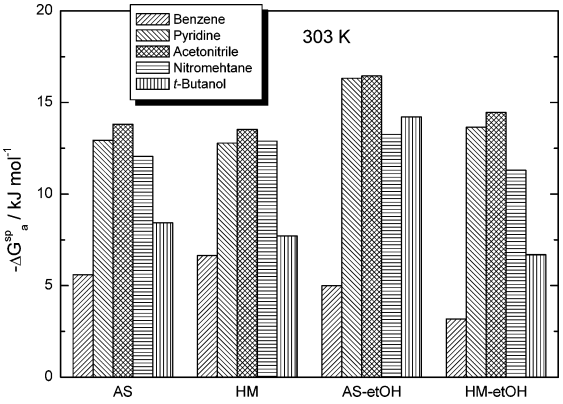

Figure 9. $-\Delta G_a^{SP}$ values calculated for the adsorption of different polar probes on the PBO surfaces under study at 303 K.

Table 9. Specific (Acid−Base) Contributions to the Standard Enthalpy of Adsorption $-\Delta H_a^{SP}$ (kJ mol^{-1}) of Several Polar Probes on PBO Surfaces

	AS	HM	AS-etOH	HM-etOH
benzene	13.1	6.7	10.0	5.3
	(3.0)	(0.9)	(1.0)	(2.3)
pyridine	35.4	18.2	19.5	20.4
	(3.7)	(1.0)	(0.5)	(2.5)
acetonitrile		19.6	34.6	27.8
		(1.2)	(1.8)	(1.2)
nitromethane	15.4	17.9	28.6	22.0
	(1.7)	(1.5)	(0.5)	(2.2)
tert-butyl alcohol	34.4	14.2	29.0	23.4
	(6.5)	(1.9)	(4.0)	(0.8)

solid surfaces in a quantitative manner. In the present work, this procedure has been discarded on an operational basis.[9]

Regarding the as-received samples, it would be rather speculative to interpret the results given that the exact formulation of the sizing is unknown. It is worth noticing, however, the strong specific interaction existing between the PBO-AS fibers and pyridine, which suggests that these fibers would exhibit the most acidic character of the four samples analyzed. This behavior also sustains the presence of residual PPA on the fiber surfaces. Washing the sizing off the PBO AS and HM samples with ethanol renders fibers with similar acid−base characteristics. Essentially, the basicity of both as-received fibers is enhanced after the cleaning process. This can be clearly observed in the case of the HM samples: the specific interaction with acidic probes (nitromethane and *tert*-butyl alcohol) increases, whereas the specific interaction with pyridine remains unchanged. For the PBO AS fibers, on the other hand, there is a big drop in the interaction with pyridine after washing the fiber, accompanied by a significant raise in the $-\Delta H_a^{SP}$ value of nitromethane; the high uncertainity of the results corresponding to the other acidic probe (*tert*-butyl alcohol) in both AS and AS-etOH samples can be misleading and should be thus taken with care. Moreover, the high specific interaction of the PBO AS sample with *tert*-butyl alcohol can be again understood in terms of the high affinity of PPA for alcohols, as mentioned before. It should be also noticed that, although the acid−base character of the AS-etOH and HM-etOH samples is quite similar, with $-\Delta H_a^{SP}$ values corresponding to the adsorption of pyridine being essentially the same for both fibers, the AS-etOH fiber shows a systematically higher interaction with the acidic probes (*tert*-butyl alcohol and, especially, nitromethane), resulting also in a higher $-\Delta H_a^{SP}$ value for the amphoteric probe (acetonitrile). This suggests that the surface of the AS-etOH fibers is slightly more basic than that of the HM-etOH samples.

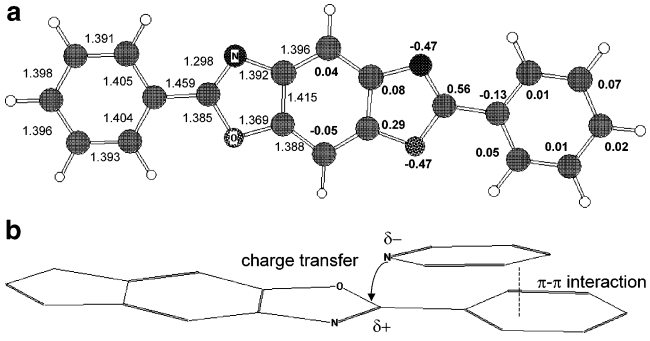

Figure 10. (a) B3YLP/6-31G* optimized structures for a partially extended PBO monomer. Distances in Å. NPA atomic charges with hydrogens summed into heavy atoms are also shown in bold characters. (b) Scheme depicting the most probable configuration of a PBO/pyridine adduct.

One interesting feature of the cleaned PBO fibers is the relatively high values of $-\Delta H_a^{SP}$ obtained for the basic probe pyridine (~20 kJ mol^{-1}). The nitrogen and oxygen atoms present in the oxazole rings are strong electron donors that should impinge a strong basic character to the PBO fibers. Obviously, the carbon atoms bonded to those electron-withdrawing groups must present an electron acceptor character that would explain to a certain extent the interaction of the macromolecules with bases. To better understand the charge distribution of the PBO, we decided to analyze the electronic and structural data of a selected model obtained from ab initio calculations. Figure 10a shows the fully B3YLP/6-31G* optimized geometry (see Experimental Section) of a partially expanded PBO monomer (two phenolic rings bonded at both ends of the benzobisoxazole moiety). Optimization of the model structure rendered a planar geometry with C_{2v} symmetry. Bond distances compare reasonably well with experimental results obtained from X-ray diffraction.[2,39] As expected, the natural population analysis (NPA) atomic charges agrees with prediction in locating the negative charges in the nitrogen, oxygen, and the carbon atoms of the phenyl groups connected to the benzobisoxazole rings. Moreover, an important positive charge (+0.56 e) is located on the carbon atoms which are bonded to those electron-withdrawing groups. Interestingly, the carbon atom of the benzo group linked to the oxygen atom of the oxazole ring also has a relatively high positive charge (+0.29 e). Because of the planarity of the highly conjugated system, it is expected that the PBO backbones are prone to establish $\pi-\pi$ interactions with appropriate molecules. Indeed, that type of interaction amounts to 5−10 kJ mol^{-1} as measured from the elution of benzene (Table 9). In the case of a highly polarized molecule such as pyridine, the above-mentioned, more exoergic interaction of approximatley 20 kJ mol^{-1} is found due to additional charge transfer and electrostatic interactions. The pyridine molecule should be thus oriented to maximize both $\pi-\pi$ and donor−acceptor charge-transfer interactions with PBO. The optimum conformation of a PBO/pyridine adduct would be more likely as shown in Figure 10b, with $\pi-\pi$ interactions being established in a parallel displaced fashion.[40]

4. Conclusion

The use of IGC combined with other techniques such as thermogravimetric analysis and AFM provided a rather detailed insight into the surface properties of PBO fibers. It was found that the sizing or finish substances present on the PBO HM variety, which strongly reduce its surface energy, can be successfully removed using ethanol or acetone; hexane is able to wipe only partially the coating off these fiber surfaces. In the case of PBO AS fibers, only washing with ethanol affects the surface properties of the fibers. Experimental results seem to agree in detecting significant amounts of contaminants that would have been originated during the fiber processing of the as-spun fibers. According to the fabrication route of PBO, these contaminants would be ascribed to PPA or partially coagulated PPA/PBO residuals. Thermal treatment at high temperatures (to obtain the high modulus variety) or washing with highly polar solvents (such as ethanol) is able to remove these contaminants, which, on the other hand, determine the surface properties of the PBO AS varieties. As a consequence, the effect (or even the existence) of an additional coating applied to the PBO AS fibers during the latter stages of their fabrication could not be unequivocally discerned. Comparison of "cleaned" fibers after ethanol washing renders significant differences between the AS and HM fibers. The former variety shows a large enhancement of the adsorption energetics of alkanes, typically related to the existence of porosity or voids at the fiber surfaces. This is not the case of the PBO HM samples. AFM measurements performed on these clean surfaces revealed a fibrillar microstructure typical of the studied rigid-rod polymer-based fibers, with fibrils being wider in the case of the heat-treated HM variety. Regarding the surface chemistry, IGC studies of the elution of probes with different donor−acceptor character confirmed the relatively high acidic character of the PBO AS fibers, which agrees with the existence of PPA residuals on their surface. Both as-spun and high-modulus PBO fibers exhibit a predominantly basic character after the cleaning process carried out with ethanol. The clean fibers, however, present also an important interaction with basic probes such as pyridine. Ab initio calculations confirmed the existence of presence of positively charged carbon atoms in the PBO monomers which should act as electron acceptors. Finally, PBO fibers are prone to exert important $\pi-\pi$ interactions as it was found both experimentally (relatively high $-\Delta H_a^{SP}$ values of benzene) and theoretically.

Acknowledgment. Financial support from the European Union (Project Growth G1RD-CT-2002-00747), 3rd PRI Asturias (Project PB-EXP01-06), and MCYT (Project MAT 2002-00041) is gratefully acknowledged. PBO samples were kindly provided by Toyobo (Japan). XPS measurements were carried out at Instituto Rocasolano (CSIC) by Dr. M. Gracia. Personal grants from The Spanish Ministry of Education (S.V.-R.) and FICYT (K.T.-M.) are also acknowledged.

References and Notes

(1) Kumar, S. In *Encyclopedia of Composites*; Lee, S. M., Ed.; VCH: New York, 1990; Vol 4, p 51.
(2) Adams, W. W., Eby, R. K., McLemore, D. E., Eds.; *The Materials Science and Engineering of Rigid-Rod Polymers*; MRS Symposium Proceedings 134; Materials Research Society: Pittsburgh, PA, 1989.
(3) Jiang, H.; Adams, W. W.; Eby, R. K. In *Handbook of Fiber Science and Technology: High Technology fibers*; Lewin, M., Preston, J., Mark, H. F., Eds.; Marcel Dekker: New York, 1996; p 171.
(4) Wolfe, J. F.; Arnold, F. E. *Macromolecules* **1981**, *14*, 909−915.
(5) Huang, Y. K.; Frings, P. H.; Hennes, E. *Composites B* **2002**, *33*, 109−115.
(6) Kumar, S.; Dang, T. D.; Arnold, F. E.; Bhattacharyya, A. R.; Min, B. G.; Zhang, X.; Vaia, R. A.; Park, C.; Adams, W. W.; Hauge, R. H.; Smalley, R. E.; Ramesh, S.; Willis, P. A. *Macromolecules* **2002**, *35*, 9039−9043.
(7) de Lange, P. J.; Mahy, J. W. G. *Fresenius J. Anal. Chem.* **1995**, *353*, 487−493.
(8) Bascom, W. D. In *Engineered Materials Handbook*; ASM International: Metals Park, OH, 1987; Vol. 1, p 122.
(9) Van Asten, A.; van Veenendaal, N.; Koster, S. *J. Chromatogr. A* **2000**, *888*, 175−196.
(10) Chan, C.-M.; Ko, T.-M.; Hiraoka, H. *Surf. Sci. Rep.* **1996**, *24*, 1−54.
(11) Bosse, F.; Schreiber, H. P.; Eisenberg, A. *Macromolecules* **1993**, *26*, 6447−6454.
(12) Mukhopadhyay, P.; Schreiber, H. P. *Macromolecules* **1993**, *26*, 6391−6396.
(13) Glass, A. S.; Larsen, J. W. *Macromolecules* **1993**, *26*, 6354−6358.
(14) Wang, J. Y.; Charlet, G. *Macromolecules* **1993**, *26*, 2413−2419.
(15) Lloyd, D. R., Ward, T. C., Schreiber, H. P., Pizaña, C. C., Eds.; *Inverse Gas Chromatography. Characterization of Polymers and Other Materials*; ACS Symposium Series 391; American Chemical Society: Washington, DC, 1989.
(16) Conder, J. R.; Young, C. L. *Physicochemical Measurements by Gas Chromatography*; Wiley: Chichester, 1979.
(17) James, P. J.; Antognozzi, M.; Tamayo, J.; McMaster, T. J.; Newton, J. M.; Miles, M. J. *Langmuir* **2001**, *17*, 349−360.
(18) Gaussian 98, Revision A.6: Frisch, M. J.; Trucks, G. W.; Schlegel, H. B.; Scuseria, G. E.; Robb, M. A.; Cheeseman, J. R.; Zakrzewski, V. G.; Montgomery, J. A.; Stratmann, R. E., Jr.; Burant, J. C.; Dapprich, S.; Millam, J. M.; Daniels, A. D.; Kudin, K. N.; Strain, M. C.; Farkas, O.; Tomasi, J.; Barone, V.; Cossi, M.; Cammi, R.; Mennucci, B.; Pomelli, C.; Adamo, C.; Clifford, S.; Ochterski, J.; Petersson, G. A.; Ayala, P. Y.; Cui, Q.; Morokuma, K.; Malick, D. K.; Rabuck, A. D.; Raghavachari, K.; Foresman, J. B.; Cioslowski, J.; Ortiz, J. V.; Stefanov, B. B.; Liu, G.; Liashenko, A.; Piskorz, P.; Komaromi, I.; Gomperts, R.; Martin, R. L.; Fox, D. J.; Keith, T.; Al-Laham, M. A.; Peng, C. Y.; Nanayakkara, A.; Gonzalez, C.; Challacombe, M.; Gill, P. M. W.; Johnson, B.; Chen, W.; Wong, M. W.; Andres, J. L.; Gonzalez, C.; Head-Gordon, M.; Replogle, E. S.; Pople, J. A. *Gaussian 98*, revision A.6; Gaussian, Inc.: Pittsburgh, PA, 1998.
(19) Becke, A. D. *Exchange-Correlation Approximation in Density-Functional Theory*; Yarkony, D. R., Ed.; World Scientific: Singapore, 1995.
(20) Herhe, W. J.; Radom, L.; Pople, J. A.; Schleyer, P. v. R. *Ab Initio Molecular Orbital Theory*; John Wiley & Sons: New York, 1986.
(21) Scott, A. P.; Radom, L. *J. Phys. Chem.* **1996**, *100*, 16502−16513.
(22) Montes-Morán, M. A.; Paredes, J. I.; Martínez-Alonso, A.; Tascón, J. M. D. *Macromolecules* **2002**, *35*, 5085−5096.
(23) Dorris, G. M.; Gray, D. G. *J. Colloid Interface Sci.* **1980**, *77*, 353−362.
(24) Montes-Morán, M. A.; Martínez-Alonso, A.; Tascón, J. M. D. *J. Mater. Chem.* **2002**, *12*, 3843−3850.
(25) Rouquerol, F.; Rouquerol, J.; Sing, K. *Adsorption by Powders and Porous Solids. Principles, Methodology and Applications*; Academic Press: London, 1999; p 439.
(26) De Boer, J. H. *The Dynamic Character of Adsorption*; Clarendon Press: Oxford, 1953.
(27) Jagiełło, J.; Bandosz, T.; Schwarz, J. A. *J. Colloid Interface Sci.* **1992**, *153*, 433−445.
(28) Chappell, P. J. C.; Williams, D. R. *J. Adhes. Sci. Technol.* **1990**, *4*, 7−16.
(29) Chappell, P. J. C.; Williams, D. R. *J. Colloid Interface Sci.* **1989**, *128*, 450−457.
(30) Kitagawa, T.; Yabuki, K. *J. Appl. Polym. Sci.* **2001**, *80*, 1030−1036.
(31) Everett, D. M.; Powl, J. C. *J. Chem. Soc., Faraday Trans. 1* **1976**, *72*, 619−636.

(32) López-Garzón, F. J.; Pyda, M.; Domingo-García, M. *Langmuir* **1993**, *9*, 531−536.
(33) Kitagawa, T.; Murase, H.; Yabuki, K. *J. Polym. Sci., Part B: Polym. Phys.* **1998**, *36*, 39−48.
(34) Donnet, J.-B.; Qin, R.-Y.; Wang, M.-J. *J. Colloid Interface Sci.* **1992**, *153*, 572−577.
(35) Gutmann, V. *The Donor−Acceptor Approach to Molecular Interactions*; Plenum Press: New York, 1979.
(36) Riddle, F. L.; Fowkes, F. M. *J. Am. Chem. Soc.* **1990**, *112*, 3259−3264.
(37) Panzer, U.; Schreiber, H. P. *Macromolecules* **1992**, *25*, 3633−3637.
(38) Donnet, J. B.; Park, S. J.; Balard, H. *Chromatographia* **1991**, *31*, 434−440.
(39) Tashiro, K.; Yoshino, J.; Kitagawa, T.; Murase, H.; Yabuki, K. *Macromolecules* **1998**, *31*, 5430−5440.
(40) Hobza, P.; Selzle, H. L.; Schlag, E. W. *J. Phys. Chem.* **1996**, *100*, 18790−18794.

MA034522L